Trade wind cumuli statistics in clean and polluted air over the Indian Ocean from in situ and remote sensing measurements

Greg M. McFarquhar,[1] Steven Platnick,[2] Larry Di Girolamo,[1] Hailong Wang,[1] Gala Wind,[3] and Guangyu Zhao[1]

Received 1 May 2004; revised 25 September 2004; accepted 14 October 2004; published 9 November 2004.

[1] Relationships between trade wind cumuli coverage and aerosol concentration N_a, and between cloud optical thickness τ_c and N_a are examined using in situ and remote sensing observations acquired on 4 days within and downwind of the Indo-Asian haze. Cloud top height and cloud coverage decrease as N_a increases, whereas τ_c increases, which could be due to aerosol or meteorological effects. Clouds with horizontal sizes less than 2 km, neglected in prior studies, contribute up to 40% to cloud area, and must be considered in studies of aerosol indirect and semi-direct effects. When radiative transfer models are applied to the observations, a regional change in top of the atmosphere TOA (surface) 0.64 μm radiative forcing of approximately +6 (+7) W m^{-2} μm^{-1} associated with changes in cloud properties is found. To the degree that synoptic-scale forcings do not vary systematically as air flows south, the results may be interpreted as the dominance of semi-direct over indirect forcing within the Indo-Asian haze for the times sampled. *INDEX TERMS:* 0305 Atmospheric Composition and Structure: Aerosols and particles (0345, 4801); 0320 Atmospheric Composition and Structure: Cloud physics and chemistry; 1610 Global Change: Atmosphere (0315, 0325); 3360 Meteorology and Atmospheric Dynamics: Remote sensing; 3359 Meteorology and Atmospheric Dynamics: Radiative processes. **Citation:** McFarquhar, G. M., S. Platnick, L. Di Girolamo, H. Wang, G. Wind, and G. Zhao (2004), Trade wind cumuli statistics in clean and polluted air over the Indian Ocean from in situ and remote sensing measurements, *Geophys. Res. Lett.*, *31*, L21105, doi:10.1029/2004GL020412.

1. Introduction

[2] Clouds affected by pollution aerosols tend to have larger number concentrations than similar clouds in pristine air [e.g., *Coakley et al.*, 1987]. Assuming the liquid water paths of perturbed and unperturbed clouds are similar, increased N_a should lead to enhanced reflection of solar radiation due to larger surface areas of smaller cloud drops [*Twomey*, 1974] and suppression of drizzle [*Albrecht*, 1989] (first and second indirect effect respectively). Where significant absorption of solar radiation by carbonaceous aerosols within haze or clouds occurs [*Ackerman et al.*, 2000], warming of the cloud layer can lead to a reduction in cloud cover (semi-direct effect). The relative importance of semi-direct and indirect effects and their role in the hydrological cycle and energy budget are not well known, and therefore, our ability to represent these processes in global models is curtailed. Here, aerosol effects on the coverage and optical properties of trade wind cumuli are examined using in situ and remote sensing observations collected inside and downwind of the Indo-Asian haze.

2. Observations Over Indian Ocean

[3] The Indian Ocean Experiment (INDOEX) operated south of India during the winter monsoon. Data from four days (Feb. 24, March 4, 11, 24, 1999) are used here when the National Center for Atmospheric Research (NCAR) C-130 aircraft left Male, Republic of Maldives (4°11′N 73°32′E) and flew south at altitudes between 400 and 1000 m sampling cloud and aerosol properties in situ. Once reaching about 7°S, the C-130 ascended to between 5 and 6.5 km on the return leg along an almost identical path 2 to 4 hours later, remotely sensing cloud properties using a multi-channel radiometer (MCR), an Advanced Microwave Imaging Radiometer (AIMR) and a scanning aerosol backscatter lidar (SABL). Analysis of Advanced Very High Resolution Radiometer (AVHRR) and sun photometer data [*Ramanathan et al.*, 2001] showed that aerosol visible optical depths τ_a varied from less than 0.1 to greater than 0.3 in the south-north direction in the vicinity of these flights, representing pristine and polluted conditions.

[4] N_a, measured by a Thermo-Systems Inc. 3760 counter, with a size threshold of 0.013 μm, is used to classify clouds as pristine ($N_a < 500$ cm^{-3}), transition ($500 < N_a < 1500$ cm^{-3}), and polluted ($N_a > 1500$ cm^{-3}) [*Heymsfield and McFarquhar*, 2001]. Because N_a does not vary significantly in the period between the outbound and return leg of the C-130, latitude divisions between pollution regimes derived from the lower altitude leg can be applied to the higher leg. Chemical analysis of samples collected during INDOEX and observations of aerosol single-scattering albedo ω_0 [*Ramanathan et al.*, 2001] at 0.53 μm showed that soot contributed to between 9 and 13% of τ_a in polluted air.

[5] Satellite images[1] show no large-scale systems over the flight tracks. Products from the National Center for Environmental Prediction (NCEP) show north-easterly (Feb. 24, Mar. 4, Mar. 24) and north-westerly 925 hPa winds (Mar. 11) in polluted air and north-westerly (Feb. 24, Mar. 11) and westerly (Mar. 4, Mar. 24) winds in pristine

[1]Department of Atmospheric Sciences, University of Illinois, Urbana, Illinois, USA.
[2]Laboratory for Atmospheres, NASA Goddard Space Flight Center, Greenbelt, Maryland, USA.
[3]L3 Communications, Government Services, Inc., Vienna, Virginia, USA.

0094-8276/04/2004GL020412$05.00

[1]Auxiliary material is available at ftp://ftp.agu.org/apend/gl/2004GL020412.

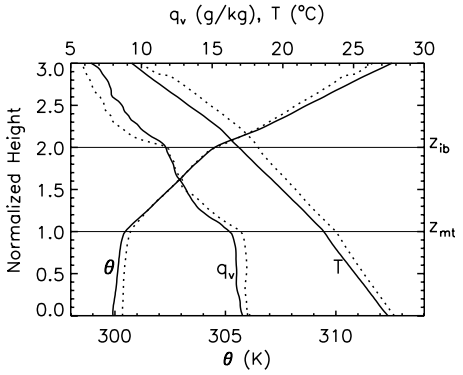

Figure 1. Average profile of potential temperature θ, T, and q_v derived from dropsondes released in polluted (dotted) and pristine (solid) conditions.

air. Surface pressure varied by less than 2 hPa over the domain and sea surface temperatures (SSTs) from the TRMM microwave imager (see auxiliary figures) varied from 29.0 ± .6°C in clean to 29.5 ± .5°C in polluted air, where uncertainties are standard deviations over the domain. For a ±10° longitude band centered on the flight tracks, NCEP mean temperatures (see auxiliary figures) T varied from 26.7 ± .7, 21.1 ± .8 and 16.7 ± .8°C at 1000, 925 and 850 hPa for clean to 27.0 ± .5, 21.7 ± .9 and 17.3 ± .9°C for polluted air and differ in a statistically significant manner according to Mann-Whitney tests. Similar tests show mean vertical velocity ω and horizontal wind u (see auxiliary figures) are identical at a 95% confidence level except for ω at 1000 hPa and u at 925 hPa. Tests also show that specific humidities (see auxiliary figures) are significantly different, with means of 13 ± 1 (12 ± 2) g kg^{-1} for clean (polluted) air at 925 hPa and 10 ± 1 (8 ± 1) g kg^{-1} at 850 hPa. Similar values of 17 ± 1 and 17 ± 1 g kg^{-1} exist at 1000 hPa.

[6] Figure 1 shows thermodynamic profiles for pristine and polluted air acquired by merging all dropsondes following *Albrecht et al.* [1995] where altitude is normalized in terms of the mixed layer top (z_{mt}) and inversion base (z_{ib}). Mann-Whitney tests show statistically similar lifting condensation levels for clean (936 ± 17 hPa) and polluted (937 ± 21 hPa) air. Precipitable water, PW, below z_{mt} is larger in clean (0.99 ± .15 cm) than polluted air (0.90 ± .14 cm), with the Mann-Whitney test only rejected at a 0.07 level. Between z_{mt} and z_{ib}, PW is statistically similar (clean: 1.4 ± .7 cm; polluted 1.3 ± .7 cm). Higher vapor mixing ratio q_v but lower PW below z_{mt} for polluted air is due to an average decrease of 60 m in z_{mt} for polluted air. This lower PW in polluted air is inconsistent with trends from large-scale NCEP analysis, but represents a more direct local measure at cloud location. The average increase in T of 0.4 to 0.7°C in the cloud layer and drier air for polluted conditions might be caused by absorption of solar radiation, preventing cloud formation through local heating effects, decreasing the boundary layer height, stabilizing the boundary layer, and feeding back on sensible and latent heat flux. However, air coming off the subcontinent may be drier than air downwind, even without aerosol forcings. Thus, findings on the importance of aerosols must be interpreted in terms of any covariability between meteorological and aerosol forcing on synoptic scales.

[7] In situ cloud observations show that average liquid water contents, LWCs, differ by less than 10% between pristine and polluted clouds, whereas average cloud drop concentrations are 3.5 times larger in polluted clouds [*Heymsfield and McFarquhar*, 2001]. The average total cross-sectional areas of drops per unit volume, proportional to extinction coefficient β_e at visible wavelengths λ, increase from 12.9 to 20.0 $mm^2 l^{-1}$ from pristine to polluted clouds. For clouds with horizontal sizes larger than 2 km, *Liu et al.* [2001] used combinations of AIMR and MCR data to show that cloud drop numbers were smaller and drop sizes and the vertical integral of LWC higher in pristine air south of 5°S compared to the polluted air north of 5°N, suggesting a first indirect effect. However, since AIMR has a coarser resolution (2 km) than MCR, properties of clouds smaller than 2 km were not considered.

[8] During INDOEX, the MCR scanned ±45° of nadir with a horizontal resolution of about 30 m depending on the C-130 altitude. The reflected radiance in a visible channel is primarily a function of τ_c. The 0.64 μm MCR radiances are converted to τ_c using routines developed for the Moderate Resolution Imaging Spectroradiometer (MODIS) Airborne Simulator that has spectral channels similar to MCR and whose retrievals of marine stratocumulus have been validated. Standard algorithms also use shortwave infrared (SWIR) water absorbing bands to retrieve drop effective radius (r_e). Unfortunately, SWIR bands had a calibration bias resulting in anomalously small r_e, precluding their use. However, the 0.64 μm radiances were deemed reasonable and useful for assessing $\Delta\tau_c$. A constant cloud top pressure of 900 mb and an above-cloud PW of 1.8 cm are used for retrieval of atmospheric corrections, consistent with observed profiles. All retrievals were visually inspected to remove areas contaminated by sun glint or underlying atolls.

[9] Three-dimensional radiative simulations, conducted with a Monte Carlo model, using observed cumuli sizes and τ_c as input, suggest that τ_c are underestimated due to side-leakage of photons. Underestimates are greater for the small sizes of trade wind cumuli than for larger cloud sizes. However, the simulations showed that retrievals of τ_c for pristine and polluted clouds could be compared in a meaningful way provided that the different populations had similar horizontal aspect ratios. MCR observations show a median aspect ratio of 1.49 for pristine clouds and 1.53 for polluted clouds.

3. Analysis of Observations

[10] Figure 2 shows the fractional area covered by different size clouds in pristine and polluted conditions. The area imaged by the MCR on all 4 days for pristine and polluted conditions is 2.3 × 10^4 and 2.2 × 10^4 km^2 respectively. A group of adjacent pixels each with τ_c greater than 2 constitutes a cloud for this analysis. Cloud diameter is defined as the area-equivalent diameter, and differs from the maximum diameter because of the aforementioned aspect ratios. In Figure 2, the fractional coverage is 8.5% for pristine clouds and 5.6% for polluted clouds. Clouds with diameters smaller than 2 km, not considered in previous studies [*Liu et al.*, 2003], contribute about 40% of the cloud area. Although quantitative results are sensitive to the threshold τ_c (2 or 3) used to define cloud and to methods used to determine a qualifying group (4 versus

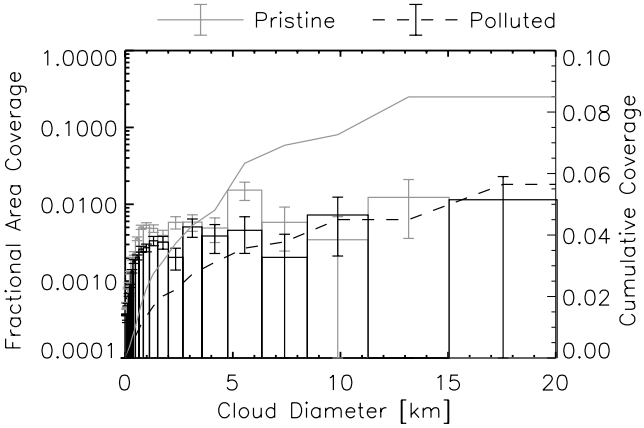

Figure 2. Fractional area coverage as function of cloud diameter for pristine (grey) and polluted (black) conditions. Solid and dashed lines represent cumulative coverage. Vertical bars represent uncertainty estimate for each bin.

8-neighbor connected), qualitative trends are identical. Day-to-day variations in cloud cover occur with fewer clouds observed on Mar. 4, but less cloud coverage is consistently noted for polluted conditions on each day.

[11] Polluted clouds were sampled 2 to 4 hours later than pristine clouds, suggesting a diurnal cycle could affect any comparison. For example, *Brill and Albrecht* [1982] observed decreases in boundary layer cloud cover after noon local time suggesting the aerosol induced reduction in cloud cover inferred from our observations may be an overestimate. However, both *Betts et al.*'s [1995] observations and *Ackerman et al.*'s [2000] modeling studies suggest that the largest decreases in cloud cover occur before noon local time, when the remote sensing observations started.

[12] The uncertainty estimates on fractional area are assumed proportional to the square root of the number of clouds sampled within the given diameter range multiplied by fractional cloud coverage. Very few large clouds were sampled, hence coverage statistics for clouds larger than 5 to 10 km are not reliable.

[13] To estimate CRF, information on the coverage for these larger clouds is needed. The needed larger sampling areas are obtained from instruments such as the Multi-Angle Imaging SpectroRadiometer (MISR). Since data are not available for 1999, swaths from MISR during February 2001–2003 in a geographic box consistent with the gradient flight location (5°N to 8°S, 68°E to 77°E) are used. Five scenes dominated by trade wind cumuli and the absence of larger-scale cloud systems are selected for analysis. MISR retrievals of τ_a suggest that polluted air masses extend further south in these years, consistent with claims that a weaker cross-equatorial flow transported less pollution to the southern hemisphere in 1999 [*Verver et al.*, 2001]. Thus, MISR data were only used to assess the contributions of larger clouds to cloud cover regardless of pristine or polluted conditions.

[14] Figure 3 shows cumulative cloud cover as a function of diameter from MISR. Clouds with diameters smaller than 5 km represent 45% of observed clouds, compared to 75% for pristine clouds and 62% for polluted clouds as observed from the MCR during INDOEX. The observed MCR trend of fewer small clouds with increased pollution is consistent

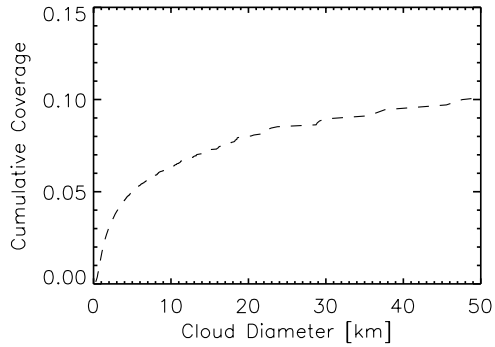

Figure 3. Cumulative cloud fraction as function of cloud diameter derived from 250 m MISR nadir camera; clouds larger than 50 km contribute an extra 0.03 to cumulative cloud fraction.

with smaller clouds and increased τ_a observed during the MISR period compared to the INDOEX period. The lower cumulative cloud coverage in polluted regions of 8.5% from MCR compared to 13% from MISR is expected given the much smaller pixel sizes of the MCR.

4. Impacts for Cloud Radiative Forcing

[15] To estimate CRF, the dependence of τ_c on cloud size is quantified. In Figure 4, no significant difference in τ_c between pristine and polluted clouds is noted for clouds with diameters less than 1 km because the smallest τ_c dominate such small sizes. For bigger clouds, where larger τ_c are more prevalent, τ_c for polluted clouds are 75% larger than for pristine clouds. Averaged over all cloud sizes and weighted according to the fractional area of each size, polluted clouds have τ_c 56% higher than pristine clouds, which may be indicative of an indirect effect and is consistent with the observed 3.5 factor increase in drop concentration. However, uncertainty estimates are significant given limited retrievals of clouds with large τ_c.

[16] An additional investigation determined how the physical thickness of clouds varied depending on N_a. During the high altitude legs, a nadir-pointing SABL measured the heights of cloud tops. Although SABL was

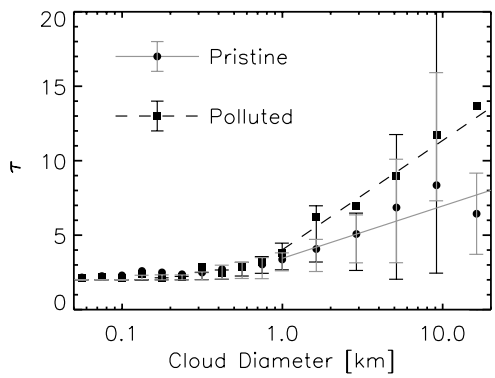

Figure 4. τ_c from MCR as function of cloud diameter for pristine and polluted conditions. Dots represent average τ_c and vertical bars run from first to third quartile of τ_c distribution for each bin. Solid/dashed lines represent best fit to data for cloud sizes larger than 1 km.

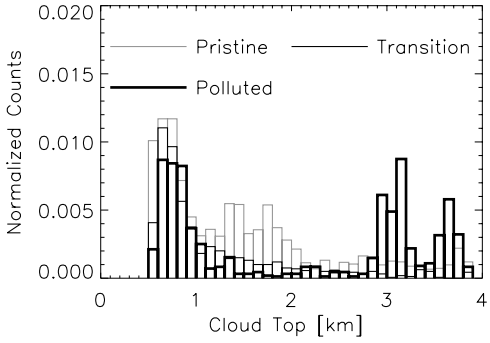

Figure 5. Frequency of occurrence of cloud top, from SABL, for pristine, transition and polluted conditions.

occulted before penetrating most trade wind cumuli, cloud base was estimated by computing the lifting condensation level from the dropsonde profiles; cloud base did not vary significantly between pristine and polluted conditions and averaged 650 m. Figure 5 shows the normalized frequency of occurrence of cloud top height. Excluding clouds with tops higher than 2 km coming from two larger cloud systems sampled in polluted air on Feb. 24 and Mar. 24, cloud tops for pristine clouds are higher than for polluted clouds, with averages of 1250 m and 1050 m respectively, suggesting typical thicknesses of 600 to 400 m.

[17] This difference in tops between pristine and polluted clouds is consistent with shallow convection gradually deepening with fetch across warm water as well as suppression of cloudiness by a semi-direct effect [*Ackerman et al.*, 2000] that would cause a decrease in boundary layer height for polluted conditions. Since adiabatic lifting models [*Brenguier et al.*, 2003] show τ_c varies with cloud thickness to 5/3 power, this difference in cloud top suggests pristine clouds should have τ_c 27% greater than polluted clouds taking into account differences in β_e observed in situ. Remote sensing observations show polluted clouds have τ_c 1.56 times greater than pristine clouds. This difference results from variations in cloud base, from differences in cloud populations sampled by the nadir-pointing SABL and the scanning MCR, from in situ extinction sampling, or from the inapplicability of the non-entrainment assumption in the adiabatic lifting model.

[18] CRF is calculated for pristine and polluted conditions for these 4 case studies using a radiative transfer model. The TOA and surface fluxes are estimated using the average τ_c for each cloud size in pristine and polluted conditions (Figure 4) using a plane-parallel model; direct absorption of solar radiation by soot is not included in the calculations in order to focus on effects from changing cloud properties. The total flux is calculated by weighting these fluxes by the fractional area covered by clouds of each size, which when compared against clear sky calculations, gives shortwave CRF. For λ of 0.64 μm, identical to that at which τ_c was retrieved, a CRF of -42 W m^{-2} μm^{-1} at the TOA and -45 W m^{-2} μm^{-1} at the surface are obtained for pristine clouds, and of -36 W m^{-2} μm^{-1} and -38 W m^{-2} μm^{-1} for polluted clouds. The change in CRF corresponding to this forcing is +6 (+7) W m^{-2} μm^{-1} at the TOA (surface). Because CRF is less negative for polluted clouds, the reduced cloud cover and liquid water path counteract the indirect effect locally. Including absorption of solar radiation by aerosols in the polluted calculations with τ_a 0.37 and ω_0 0.89, the TOA (surface) CRF becomes -35 (-44) W m^{-2} μm^{-1}, corresponding to a change of CRF associated with aerosols of +7 (+1) W m^{-2} μm^{-1}. If we assume that 0.64 μm is representative of all λ, then the change in broadband CRF is +6 (+.85) W m^{-2}, obtained by multiplying by the total solar flux of 1370 W m^{-2} and dividing by the 0.64 μm irradiance of 1622 W m^{-2} μm^{-1}. The change in surface CRF is dependent on the assumed τ_a. Correlated and uncorrelated variations in meteorology, thermodynamic fluxes, and an observed diurnal cycle may naturally cause variations in cloud cover between pristine and polluted regions that would also affect the estimates of CRF.

[19] **Acknowledgments.** The National Aeronautics and Space Administration Global Water and Energy Cycle Research and Analysis Program and the Jet Propulsion Laboratory supported this research. Findings do not necessarily represent their views. Dropsonde and MCR data were obtained from NCAR's Joint Office of Science Support, SABL data from the Atmospheric Technology Division of NCAR and MISR data from the Langley DAAC. J. Coakley was PI for MCR and A. Heymsfield for SABL. The advice or assistance of M. Tschudi, F. Evans, T. Varnai, K. Middleton, D. Bramer, J. Birky, J. L. Brenguier and an anonymous reviewer were appreciated.

References

Ackerman, A. S., O. B. Toon, D. E. Stevens, A. J. Heymsfield, V. Ramanathan, and E. J. Welton (2000), Reduction of tropical cloudiness by soot, *Science*, *288*, 1042–1047.

Albrecht, B. A. (1989), Aerosols, cloud microphysics, and fractional cloudiness, *Science*, *245*, 1227–1230.

Albrecht, B. A., M. P. Jensen, and W. J. Syrett (1995), Marine boundary layer structure and fractional cloudiness, *J. Geophys. Res.*, *100*, 14,209–14,222.

Betts, A. K., C. S. Bretherton, and E. Klinker (1995), Relation between mean boundary-layer structure and cloudiness at the R/V *Valdivia* during ASTEX, *J. Atmos. Sci.*, *52*, 2752–2759.

Brenguier, J., H. Pawlowska, and L. Schüller (2003), Cloud microphysical and radiative properties for parameterization and satellite monitoring of the indirect effect of aerosol on climate, *J. Geophys. Res.*, *108*(D15), 8632, doi:10.1029/2002JD002682.

Brill, K., and B. Albrecht (1982), Diurnal variation of the trade-wind boundary layer, *Mon. Weather Rev.*, *110*, 601–613.

Coakley, J. A., Jr., R. L. Bernstein, and P. A. Durkee (1987), Effect of ship-stack effluents on cloud reflectivity, *Science*, *237*, 1020–1022.

Heymsfield, A. J., and G. M. McFarquhar (2001), Microphysics of INDOEX clean and polluted trade cumulus clouds, *J. Geophys. Res.*, *106*, 28,653–28,673.

Liu, G., J. A. Curry, J. A. Haggerty, and Y. Fu (2001), Retrieval and characterization of cloud liquid water path using airborne passive microwave data during INDOEX, *J. Geophys. Res.*, *106*, 28,719–28,730.

Liu, G., H. Shao, J. A. Coakley Jr., J. A. Curry, J. A. Haggerty, and M. A. Tschudi (2003), Retrieval of cloud droplet size from visible and microwave radiometric measurements during INDOEX: Implication to aerosols' indirect radiative effect, *J. Geophys. Res.*, *108*(D1), 4006, doi:10.1029/2001JD001395.

Ramanathan, V., et al. (2001), Indian Ocean Experiment: An integrated analysis of the climate forcing and effects of the great Indo-Asian haze, *J. Geophys. Res.*, *106*, 28,371–28,398.

Twomey, S. (1974), Pollution and the planetary albedo, *Atmos. Environ.*, *8*, 1251–1256.

Verver, G. H. L., D. R. Sikka, J. M. Lobert, G. Stossmeister, and M. Zachariasse (2001), Overview of the meteorological conditions and atmospheric transport processes during INDOEX 1999, *J. Geophys. Res.*, *106*, 28,399–28,413.

L. Di Girolamo, G. M. McFarquhar, H. Wang, and G. Zhao, Department of Atmospheric Sciences, University of Illinois, 105 S. Gregory Street, Urbana, IL 61801, USA. (mcfarq@atmos.uiuc.edu)

S. Platnick, Laboratory for Atmospheres, NASA Goddard Space Flight Center, Code 913, Bldg 33, Rm A305, Greenbelt, MD 21114, USA.

G. Wind, L3 Communications, Government Services, Inc., Vienna, VA 22180, USA.